ISBN: 978-3-95450-249-3 ISSN: 2673-5350 doi: 10.18429/JACoW-IBIC2024-WEP17

PHYSICAL DESIGN OF AN ONLINE BEAM MONITOR FOR HEAVY-ION SINGLE EVENT EFFECTS

D. Wang†, W. Chen, Z. M. Wang, M.W. Wang, Y. H. Yan, B. C. Wang
National Key Laboratory of Intense Pulsed Radiation Simulation and Effect, Northwest Institute of Nuclear Technology, Xi'an, China

Abstract

Accurate measurement of flux rate is essential in heavy-ion single event effects tests, but it presents significant challenges for monitoring low energy (5~10 MeV/u) and low intensity (less than 1E6 /s) heavy-ion beams. In this paper, we propose a novel detector that enables real-time monitoring of flux rate by simultaneously measuring the beam intensity and profile using secondary electrons on both the front and back surfaces of thin foils. The confinement of secondary electrons through electric and magnetic fields is achieved, with CST simulation has been utilized to validate the method. This approach offers several advantages over conventional methods, including high space and time resolution, reduced mass thickness, and multi-parameter measurement capability.

INTRODUCTION

Single event effects (SEE) of integrated circuits are one of the main threats faced by spacecrafts, and heavy-ion accelerators are commonly used for SEE studies on Earth. As per the European guidelines for SEE tests [1], it is recommended that the heavy-ion flux rate be less than 1E5 /(cm^2·s), which corresponds to a maximum beam intensity of several hundred femtoamperes. Limited by the scale of general accelerators, the energy of heavy ions with higher Linear Energy Transfer (LET) values can typically only reach several MeV/u. Irradiation tests of Device Under Tests (DUTs) with heavy-ion beams are generally conducted in a vacuum environment.

In irradiation experiments, the parameters of greatest concern to users are the flux rate and its uniformity at the irradiation terminal. Therefore, real-time, direct measurement of these key parameters during the irradiation process is essential. However, online monitoring of low-energy heavy-ion beams presents considerable challenges, and commonly used detectors such as parallel ionization chambers, semiconductors, and scintillators are no longer suitable for use as non-destructive beam monitors [2].

Measuring the secondary electrons (SEs) produced by heavy ions penetration through thin foils on their surfaces is a potential solution. Due to the fact that the thickness of the thin foil is significantly smaller than the range of ions, it can serve as a non-interceptive beam monitor, named secondary emission for low-interception monitoring (SLIM). Additionally, employing Microchannel Plates (MCPs) to multiply the SEs enables measurement of low-intensity beams. Previous research on SLIM has primarily focused on utilizing single-sided SEs for profiling, beam intensity measurements, or timing analysis. This type of detector demonstrates excellent time resolution and space resolution [3-8].

PHYSICAL DESIGN

This paper introduces a novel SLIM structure that utilizes SEs emitted from front and back surfaces of the thin foil to simultaneously measure beam intensity and profile distribution, enabling online monitoring of dose rate.

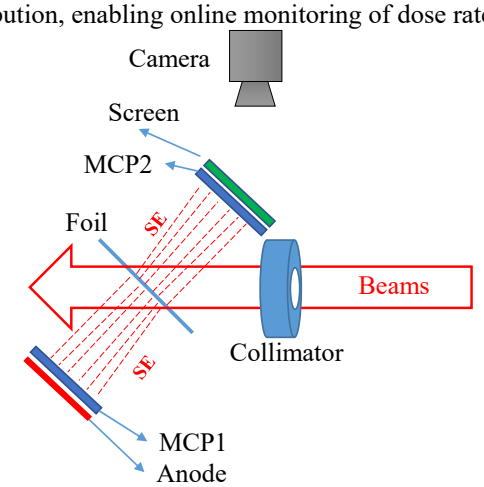

Figure 1: Conceptual illustration of the SLIM.

The thin foil is oriented at a 45° angle relative to the beam axis, with one MCP assembly positioned on each side of the foil surface (Fig. 1). The electric signal from the anode of the forward MCP1 assembly is utilized to measure the beam intensity, whereas the light signal from the fluorescent screen of the backward MCP2 assembly is employed to assess the beam profile. Concurrently, based on the beam intensity and profile distribution, the dose rate and uniformity at various positions can be acquired. H.Rothard have investigated the generation of SEs on both the front and back surfaces of thin foils [9]. The findings indicate that a greater number of SEs are produced in the forward direction compared to the backward direction. Consequently, the measurement of weak current signals should be preferentially set in the forward direction.

The confinement of SEs is a key issue due to their initial emission angle distribution. The traditional SLIM utilizes a wire mesh near the thin foil surface to create an accelerating electric field, enabling accelerated SEs to quickly reach the MCP entrance surface and reduce lateral diffusion. However, this structure has a defect in that approximately 5% to 10% of the particles will be stopped by the wire due to its comparable diameter with the range of low-

† wangdi@nint.ac.cn

ISBN: 978-3-95450-249-3 ISSN: 2673-5350 doi: 10.18429/JACoW-IBIC2024-WEP17

energy heavy ions. Additionally, the drastic change in electric field near the wire results in poorer space resolution at its corresponding position.

Therefore, this article abandons the use of wire mesh and only applies negative high voltage to the thin foil. By utilizing the potential difference between the thin foil and MCP entrance surface, the SEs are accelerated. Besides, permanent magnets are introduced with its polarization di rection perpendicular to the foil surface, see Fig. 2.

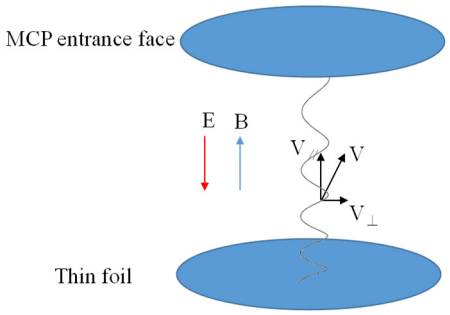

Figure 2: Diagram of a constrained electron.

We can decompose the electron velocity $\boldsymbol{v}$ into two com ponents,

$$\boldsymbol{v} = \boldsymbol{v}_{\perp} + \boldsymbol{v}_{\parallel} \quad (1)$$

where $\boldsymbol{v}_{\perp}$ is the electron velocity perpendicular to the E-field direction, and $\boldsymbol{v}_{\parallel}$ is parallel to it. According to the laws of motion, $\boldsymbol{v}_{\perp}$ will be almost constant, while $\boldsymbol{v}_{\parallel}$ at the MCP entrance surface is much greater than the initial value. This is due to the electron energy will increase from several eV to keV under the influence of E-field. If we neglect the differences between the initial velocities, then the drift time t is only related to the E-field. Meanwhile, in the presence of the magnetic field, B, the SEs will move in a spiral as shown in Fig. 2. It can be derived that when the relation

$$qB/t = 2\pi n \quad (n = 1, 2, 3, 4, \dots) \quad (2)$$

is satisfied, the SEs will make an integer number of turns, which means the influence of electron transverse motion on space resolution is essentially eliminated. Consequently, the detector can give an as good as possible image of the foil through the coupling of electrostatic and magnetic fields.

SIMULATION AND RESULTS

Secondary electron emission induced by ions have three main characteristics. Firstly, the emission angle of SEs approximately follows a cosine distribution, meaning that the probability is highest when perpendicular to the emission surface. Secondly, the average energy of SEs is several eV, with the vast majority of energy below 50 eV. Thirdly, the yield is appropriately proportional to the ionization energy loss at surface. At present, the vast majority of popular Monte Carlo programs cannot simulate the generation process of SEs in this energy range [10]. Therefore, based on the angle and energy distribution formulas, this paper adopts the acceptance-rejection sampling method to generate SEs directly from random numbers. Figure 3 shows the angle and energy distribution of 10,000 SEs.

In Fig. 3, the angle distribution satisfies Eq. (3) where θ is the angle between the SE and the normal of the surface.

$$p(\theta) = \cos\theta \quad (3)$$

And the energy distribution proposed by P. N. Ostroumov was utilized [5]. The function is expressed by

$$p(E) = \frac{\alpha_1}{\sqrt{2\pi{\sigma_1}^2}} \exp\left[-\frac{(E-E_{c1})^2}{2{\sigma_1}^2}\right] + \frac{\alpha_2}{\sqrt{2\pi{\sigma_2}^2}} \exp\left[-\frac{(E-E_{c2})^2}{2{\sigma_2}^2}\right] + \frac{\alpha_3}{E_M} \exp\left(-\frac{E}{E_M}\right) \quad (4)$$

where the parameters used are listed in Fig. 3 (bottom).

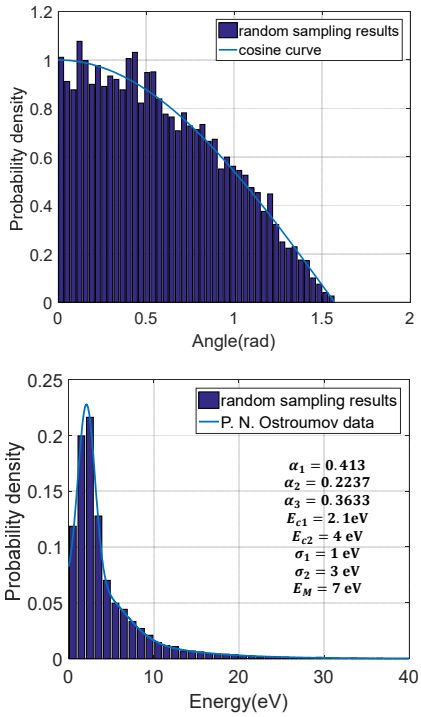

Figure 3: Angle(top) and energy(bottom) distribution by sampling compared to the probability density function [Eq. (3) and Eq. (4)].

The Particle Tracking simulation within CST Studio Suite [11] is employed to execute the trajectory simulation of electrons in fields. The particle interface files contains information such as the energy, direction, and initial position of SEs. The geometric model includes major components such as vacuum chamber, permanent magnets, foil, MCP assemblies, and support rods, as depicted in Fig. 4.

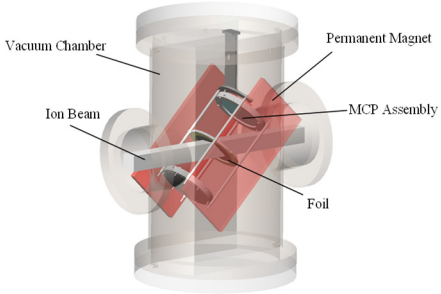

Figure 4: CST model of the SLIM.

The maximum beam size needed to be measured is 30×30 mm². Based on the MCP product model, an effective

ISBN: 978-3-95450-249-3 ISSN: 2673-5350 doi: 10.18429/JACoW-IBIC2024-WEP17

diameter of 82 mm is selected for the MCP, and for ease of assembly, the conductive thin foil also has a same diameter. While ensuring proper beam passage, efforts are made to minimize the distance between the MCP assembly and thin foil in order to enhance electric field uniformity in the central region. In this model, a distance of 85 mm is maintained. The permanent magnets, which envelop the cylindrical region bounded by two MCP assemblies, are placed on both sides of the beam.

Due to the fact that the beam spot size in the vertical direction is magnified by a factor of $\sqrt{2}$ on the foil, the beam spot area on the foil is approximately 30x42 mm^2 in simulation model. Based on the symmetry, 16 point sources are emitted within one-quarter of the beam spot area on the thin foil, as depicted in Fig. 5. Each point source emits 10,000 SEs that satisfy both angle and energy distributions. At the same time, an electron area source with the same size as beam spot is set up on the other side of the thin foil. Through these settings, we can observe the electron trajectory and imaging distribution. The trajectory plot is shown in Fig. 6, and the dispersion of the electron point sources on the MCP entrance surface is depicted in Fig. 7.

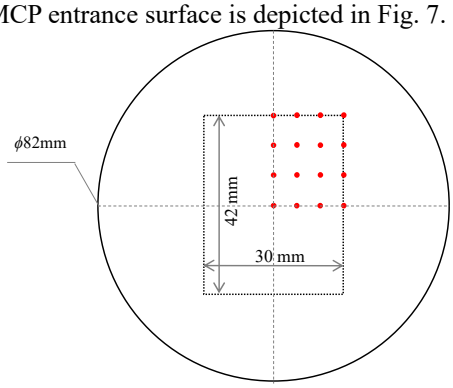

Figure 5: Schematic diagram of the point sources.

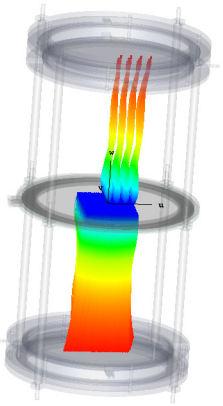

Figure 6: CST trajectory plot for the point sources and area source emitted from the front and back surfaces respectively.

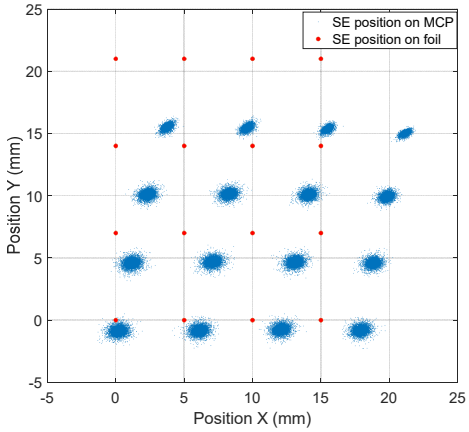

Figure 7: Position distribution on MCP compared to initial points on foil.

In the simulation, it is observed that the size of the electron spots in Fig. 7 varies with voltage, indicating that the space resolution can be adjusted by scanning the foil voltage. Besides, we can find that there is a distortion in imaging as the electron spots do not align with the original point sources, indicating that there is a distortion in the imaging, which can be corrected by position calibration. It should be noted that in a uniform magnetic field and electric field scenario, distortion would not occur; however, this ideal condition is impractical due to limitations on dimensions of permanent magnets and foil. Considering practical engineering，a permanent magnet size of 130×270×10 mm^3 with a remanence of 1 T has been selected in our model.

In order to quantify time and space resolution, firstly, the drift time of electrons arriving at the MCP entrance surface was statistically analysed, as shown in Fig. 8. Figure 9 presents the mean and standard deviation of the drift time as a function of voltage V. It can be observed that the mean time is less than 10 ns, with a standard deviation under 0.3 ns. Furthermore, both the mean and standard deviation decrease with increasing voltage. Considering that the pulse width of the MCP is approximately 0.5 ns, it can be anticipated that the time resolution of this detector will be better than 1 ns.

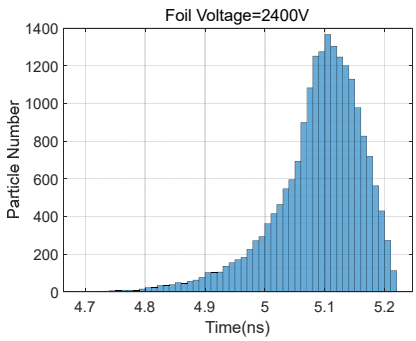

Figure 8: Distribution of the drift time when V=2400 V.

ISBN: 978-3-95450-249-3 ISSN: 2673-5350 doi: 10.18429/JACoW-IBIC2024-WEP17

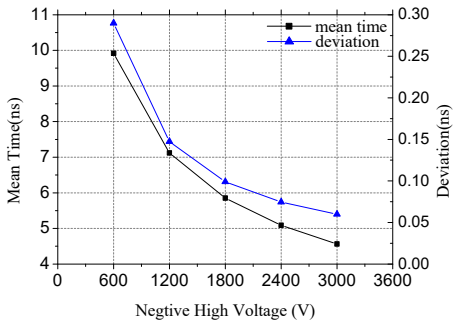

Figure 9: Mean and deviation of the drift time as a function of voltage.

Furthermore, two point sources with a spacing of 0.5 mm are emitted from the thin foil. By adjusting an appropriate foil voltage, an almost completely separate distribution on the MCP entrance surface can be achieved (Fig. 10), indicating that the space resolution is better than 0.5 mm, meeting the monitoring requirements of SEE tests adequately.

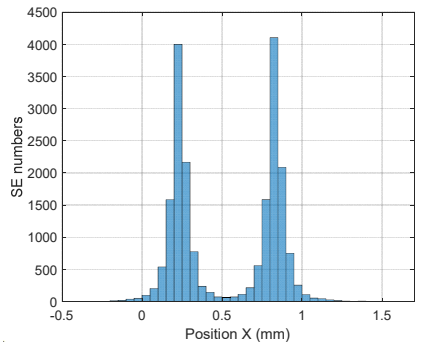

Figure 10: 1D distribution of horizontal direction.

CONCLUSIONS

This paper presents a novel approach that utilizes SEs from the front and back surfaces of a thin foil to simultaneously measure beam intensity and profile, thereby enabling online monitoring of the flux rate. This method offers several advantages over traditional monitoring techniques, including high resolution, reducedmass thickness, and the capability for multi-parameter measurements.

Additionally, by employing adjustable electrostatic fields and constant magnetic fields to constrain SEs, a configuration without an accelerating wire mesh and with lateral rectangular permanent magnets is proposed. The beam only traverses a thin layer of foil, and space resolution optimization can be achieved by adjusting the foil voltage. Simulation results show that the space resolution is better than 0.5 mm, while the time resolution is better than 1 ns.

In the future, the manufacturing and testing of the detector will be completed, providing a high-performance detector for online monitoring of low-energy and low-intensity heavy-ion beams.

REFERENCES

[1] *Single event effects test method and guidelines, ESCC Basic Specification*, European Space Agency, no. 25100, Oct. 2002.

[2] P. Strehl, *Beam Instrumentation and Diagnostics*. Berlin Heidelberg: Springer, 2006. doi:10.1007/3-540-26404-3

[3] K. Kruglov, L. Weissman, P. V. D. Bergh, A. Andreyev, M. Huyse, and P. V. Duppen, "A beam diagnostic system for low-intensity radioactive beams", *Nuclear Inst & Methods in Physics Research A*, vol. 441, pp. 595-604, 2000. doi:10.1016/S0168-9002(99)01001-3

[4] D. Shapira, T. A. Lewis and L. D. Hulett, "A fast and accurate position-sensitive timing detector based on secondary electron emission", *Nuclear Inst & Methods in Physics Research A*, vol. 454, pp. 409-420, 2000. doi:10.1016/S0168-9002(00)00499-X

[5] P. N. Ostroumov, P. Billquist, M. Portillo, and W. Q. Shen, "Design and test of a beam profile monitoring device for low intensity radioactive beams", *Review of Scientific Instruments*, vol. 73, pp. 56-62, 2002. doi:10.1016/S0168-9002(00)00499-X

[6] L. Badano, O. Ferrando, M. Pezzetta, T. Klatka, M. Koziel, and G. Molinari, "SLIM (Secondary emission monitor for Low Interception Monitoring) an innovative non-destructive beam monitor for the extraction lines of a hadrontherapy center", *2003 IEEE Nuclear Science Symposium. Conference Record* (IEEE Cat. No.03CH37515), Vol. 3, pp. 1561-1565, 2003. doi:10.1109/nssmic.2003.1352175.

[7] J. Harasimowicz, J.-L. Fernandez-Hernando, C. P. Welsch, L. Cosentino, P. Finocchiaro, and A. Pappalardo, "Thin Foil-based Secondary Emission Monitor for Low Intensity, Low Energy Beam Profile Measurements", in *Proc. IPAC'11*, San Sebastian, Spain, Sep. 2011, paper TUPC162, pp. 1413-1415.

[8] T. Liu, R. Mao, Y. Yuan, C. Huang, L. Yao, Z. Xu, P. Li, Y. Feng, Y. You, and H. Yang, "Performance of the secondary electrons profile monitor for the scanning gantry in the heavy ion medical machine", *Nuclear Instruments and Methods in Physics Research Section A: Accelerators, Spectrometers, Detectors and Associated Equipment,* vol. 999, p. 165212, 2021. doi: 10.1016/j.nima.2021.165212

[9] Rothard, Kroneberger, Clouvas, Veje, Lorenzen, Keller *et al.*, "Secondary-electron yields from thin foils: A possible probe for the electronic stopping power of heavy ions", *Physical review. A*, vol. 41, pp. 2521-2535, 1990. doi: 10.1103/PhysRevA.41.2521

[10] Q. Gibaru, C. Inguimbert, P. Caron, M. Raine, D. Lambert, and J. Puech, "Geant4 physics processes for microdosimetry and secondary electron emission simulation: Extension of MicroElec to very low energies and 11 materials (C, Al, Si, Ti, Ni, Cu, Ge, Ag, W, Kapton and SiO2)", *Nuclear Instruments and Methods in Physics Research Section B: Beam Interactions with Materials and Atoms*, vol. 487, pp. 66-77, 2021. doi: 10.1016/j.nimb.2020.11.016

[11] CST Studio Suite, www.cst.com